BIOLOGICAL SCIENCES: Microbiology

A specific non-bisphosphonate inhibitor of the bifunctional farnesyl/geranylgeranyl diphosphate synthase in malaria parasites

Jolyn E. Gisselberg[1], Zachary Herrera[1], Lindsey Orchard[4], Manuel Llinás[4,5,6], and Ellen Yeh[1,2,3*]

[1]Department of Biochemistry, [2]Pathology, and [3]Microbiology and Immunology, Stanford Medical School, Stanford University, Stanford, CA 94025, USA

[4]Department of Biochemistry & Molecular Biology, [5]Department of Chemistry and [6]Huck Center for Malaria Research, Pennsylvania State University, University Park, PA 16802

*Corresponding author: ellenyeh@stanford.edu

Keywords: malaria, drug discovery, and high-throughput screening, non-bisphosphonate inhibitor

Abstract

There are multiple validated antimalarial drug targets in isoprenoid biosynthetic pathways. Using a growth rescue screen, we identified MMV019313 as an inhibitor of isoprenoid biosynthesis in *Plasmodium falciparum* parasites that cause malaria. We demonstrate that the molecular target of MMV019313 is the *P. falciparum* bifunctional farnesyl and geranylgeranyl diphosphate synthase (FPPS/GGPPS): Both an S228T variant and overexpression of wildtype *Pf*FPPS/GGPPS conferred resistance to MMV019313. MMV019313 also inhibited the activity of purified *Pf*FPPS/GGPPS. *Pf*FPPS/GGPPS has already been validated as an antimalarial drug target since its inhibition by bisphosphonates, a class of drugs that inhibits human FPPS, was shown to clear parasitemia in a mouse malaria model. Though bisphosphonates are clinically used for treating osteoporosis, MMV019313 has significant advantages over bisphosphonates for antimalarial drug development. MMV019313 has superior physicochemical properties compared to charged bisphosphonates that have poor bioavailability and strong bone affinity. We also show that it is highly selective for *Pf*FPPS/GGPPS and showed no activity against human FPPS or GGPPS. Inhibition of *Pf*FPPS/GGPPS by MMV019313, but not bisphosphonates, was disrupted in the S228T variant, demonstrating that MMV019313 and bisphosphonates have distinct modes-of-inhibition against *Pf*FPPS/GGPPS. In addition, we describe two methodological improvements: a more sensitive chemical rescue screen for identifying isoprenoid inhibitors and the first report using chemical mutagenesis for drug resistance selection in *Plasmodium*. Altogether MMV019313 is the first specific, non-bisphosphonate inhibitor of *Pf*FPPS/GGPPS. Our findings uncover a new small molecule binding site in this important antimalarial drug target and provide a promising starting point for development of *Plasmodium*-specific FPPS/GGPPS inhibitors.

Significance Statement

There is an urgent need for antimalarials with novel mechanisms-of-action to circumvent resistance to frontline drugs. Isoprenoid biosynthetic pathways are essential for *Plasmodium* (malaria) parasites and contain multiple validated drug targets. We identify a new antimalarial compound that inhibits a key branchpoint enzyme in isoprenoid biosynthesis. Our compound has significant advantages over bisphosphonate inhibitors that inhibit the same drug target with improved drug properties and specificity for the *Plasmodium* enzyme over human homologs. Our findings uncover a new "druggable" site in this important antimalarial drug target and provide a chemical starting point for development of *Plasmodium*-specific FPPS/GGPPS inhibitors.

Introduction

There is an urgent need for antimalarials with novel mechanisms-of-action to circumvent resistance to frontline drugs. The biosynthesis of cellular isoprenoids is an essential process in *Plasmodium* parasites that cause malaria. A number of antimalarial compounds target enzymes in isoprenoid biosynthetic pathways leading to parasite growth inhibition. First, *Plasmodium* parasites depend on the 7-enzyme prokaryotic 2-*C*-methyl-D-erythritol 4-phosphate (MEP) pathway in its plastid organelle, the apicoplast, to produce isopentenyl pyrophosphate (IPP) and its isomer dimethyallyl pyrophosphate (DMAPP) (1). IPP and DMAPP are the C5 building blocks for all isoprenoids. The antibiotic fosmidomycin inhibits the MEP enzyme, Dxr/IspC, in both bacteria and *Plasmodium* parasites (1).

Second, at least three isoprenoid synthases (PF3D7_1128400.1, PF3D7_0202700, PF3D7_0826400) catalyze the condensation of IPP and DMAPP into longer prenyl chains (2-4).

In particular, farnesyl pyrophosphate synthase (FPPS) and geranylgeranyl pyrophosphate synthase (GGPPS) are key branch point enzymes that synthesize C15 and C20 prenyl chains, respectively, for multiple downstream enzymes. Nitrogen-containing bisphosphonates, blockbuster drugs which inhibit human FPPS, also inhibit the bifunctional FPPS/GGPPS found in *Plasmodium* parasites (5-9).

Finally, prenyl chains are cyclized and/or conjugated to small molecule and protein scaffolds by a variety of prenyltransferases to biosynthesize final isoprenoid products required for parasite growth and replication. Tetrahydroquinolines (THQ) have been shown to potently inhibit the *Plasmodium* protein farnesyltransferase (10-12). Other inhibitors may interfere with isoprenoid biosynthesis indirectly by disrupting transporters that supply starting substrates or export products or blocking pathways that provide cofactors for isoprenoid biosynthetic enzymes.

Importantly fosmidomycin, bisphosphonates, and tetrahydroquinolines have all shown efficacy in mouse models of malaria infection, validating the key importance of isoprenoid biosynthesis as an antimalarial drug target (1, 5, 6, 10). Fosmidomycin is currently being tested in human clinical trials, while a THQ lead candidate was investigated in preclinical studies (10, 13). However, novel chemical scaffolds that disrupt isoprenoid biosynthetic pathways in *Plasmodium* remain desirable to overcome unfavorable drug properties of these known inhibitors. For example, bisphosphonates avidly bind bone mineral, and both fosmidomycin and THQs have short half-lives *in vivo* (14-16).

In 2011 the Medicine for Malaria Venture (MMV) distributed the Open-Access Malaria Box to accelerate antimalarial drug discovery (17). The Malaria Box consists of 400 structurally diverse compounds, curated from >20,000 hits generated from large-scale screens, that inhibit the growth of blood-stage *Plasmodium falciparum* parasites (18-20). A major goal of sharing these compounds was to facilitate elucidation of their antimalarial mechanism-of-action and open new classes of validated chemical scaffolds and drug targets. Compounds that disrupt isoprenoid metabolism can be detected by "rescue" of their growth inhibition upon supplementation of isoprenoids in the growth media (21). Previously, we and two other groups screened the Malaria Box for compounds whose growth inhibition were rescued by addition of IPP and identified MMV008138 (22, 23). We and our collaborators demonstrated that MMV008138 inhibits IspD, an enzyme in the MEP pathway that produces IPP (23).

Using a quantitative high-throughput screen (qHTS), we report a second compound in the Malaria Box, MMV019313, that shows an IPP rescue phenotype but was not identified in screens performed by other groups (22, 24, 25). We demonstrate that the target of MMV019313 is the *P. falciparum* FPPS/GGPPS, a cytosolic isoprenoid synthase that utilizes IPP and the key branch point enzyme in isoprenoid biosynthesis in parasites. MMV019313 represents the first new class of non-bisphosphonate inhibitors of *Pf*FPPS/GGPPS.

Results

A quantitative high-throughput screen (qHTS) for growth and IPP rescue identifies MMV019313 as an inhibitor of isoprenoid biosynthesis

Previous IPP rescue screens of the Malaria Box tested compounds at a single, high concentration >5 μM (22, 24, 25). While testing compounds at a single concentration is useful for identifying phenotypes that occur at a threshold concentration (e.g. growth inhibition), growth rescue is expected to occur within a specific range of concentrations. For example,

doxycycline inhibits *P. falciparum* growth with an EC_{50}= 0.3 μM that increases to 3.2 μM upon addition of IPP (21). At concentrations <0.3 μM, doxycycline does not cause growth inhibition. However, at concentrations >3.2 μM, it is no longer specific for its target and causes growth inhibition through additional targets that cannot be IPP rescued. Therefore the concentration range in which IPP rescue can be observed is greater than the EC_{50} of the compound for its specific, IPP-rescuable target but less than that for any nonspecific targets.

To increase the sensitivity for detecting IPP chemical rescue, we screened the Malaria Box for growth inhibition of blood-stage *P. falciparum* in the presence and absence of IPP over 8-12 drug concentrations from 0.01-27 μM (Table S1). Of 397 compounds tested (3 compounds were not available), 383 showed growth inhibition at ≤27 μM. Initial hits showing IPP rescue of growth inhibition at one or more drug concentrations were commercially sourced and retested. Along with the previously reported compound, MMV008138, we confirmed a second compound in the Malaria Box showing an IPP rescue phenotype, MMV019313 (Figure 1A). MMV019313 inhibited *P. falciparum* growth measured in a single replication cycle with EC_{50}=268 nM (250-289 nM) in the absence of IPP; in the presence of IPP, the EC_{50} was over 13-fold more at 3.6 μM (3.2-4.0 μM) (Figure 1B). Notably, at concentrations >3.6 μM, MMV019313 inhibits a nonspecific target that can no longer be IPP rescued, which explains why it was not identified in previous screens.

An unusual feature of blood-stage *Plasmodium* is that IPP can rescue complete loss of the apicoplast, the plastid organelle which houses the MEP pathway, since production of IPP is the only essential function of the apicoplast. Compounds like doxycycline that disrupt apicoplast biogenesis cause growth inhibition rescued by IPP and result in parasites lacking an apicoplast (21). In contrast, inhibitors of isoprenoid biosynthesis, like fosmidomycin and MMV008138, cause growth inhibition rescued by IPP with an intact apicoplast (26). We determined whether MMV019313 disrupted the biogenesis of the apicoplast. Both the replication of the apicoplast genome and import of an apicoplast-targeted GFP were intact in MMV019313-treated and IPP-rescued parasites (Figure S1; 21). Altogether MMV019313 causes growth inhibition rescued by IPP with no defect in apicoplast biogenesis, suggesting that, like fosmidomycin and MMV008138, MMV019313 blocks isoprenoid biosynthesis (23).

MMV019313-resistant parasites contain a mutation in the geranylgeranyl diphosphate synthase

To gain further insight into the mechanism-of-action of MMV019313, we identified mutations that confer resistance to MMV019313. Our initial attempt to select drug-resistant parasites from a bulk culture of 10^{10} parasites was not successful, though this same protocol was effective in selecting drug resistance against MMV008138 when performed in parallel (23). Therefore, we turned to chemical mutagenesis to increase the likelihood of selecting MMV019313-resistant parasites. Chemical mutagenesis has been successfully employed to perform genetic screens in *T. gondii* but, to our knowledge, has not been used in *Plasmodium* parasites (27). We treated 10^8 *P. falciparum* W2 parasites with sub-lethal doses of ethyl methanesulfonate (EMS), an alkylating agent. Because EMS is unstable, we tested a fresh batch of mutagen immediately prior to treatment in a standard parasite growth inhibition assay to determine its EC_{50}. We then selected the EC_{50} as the highest mutagen concentration used and also tested several lower concentrations by serially diluting 3-fold. These concentrations were selected to maximize the frequency of drug-resistant mutations while minimizing lethal mutations that would result in a smaller pool of starting parasites or nonspecific passenger

mutations that would confound identification of causative mutations. Following mutagenesis, parasites were continuously selected with a dose of MMV019313 equal to its EC_{75} in the presence of IPP for 7 or 32 days before removal of the drug. This concentration was chosen to maximize selection pressure for developing resistance in the IPP-rescuable target, while minimizing that for developing resistance in nonspecific targets.

Resistant parasites emerged in all mutagenized cultures one week after drug removal. In these resistant populations, MMV019313 showed EC_{50} values that ranged from 3-9-fold greater than that observed in the initial susceptible population. Growth inhibition of two MMV019313-resistant populations which showed the highest levels of resistance at the lowest EMS concentrations used, designated 019313R1 and 019313R2, are shown in Figure 2A. Significantly the EC_{50} of MMV019313 in 019313R1 and 019313R2 was similar to that observed in susceptible strains in the presence of IPP, and growth inhibition could no longer be rescued by addition of IPP (Figure S2). These results suggest that, as expected, 019313R1 and 019313R2 populations were completely resistant to inhibition of its specific IPP-rescuable target but had not developed resistance to inhibition of additional nonspecific targets. This is the first example of using chemical mutagenesis to aid selection of drug-resistant parasites in *P. falciparum.*

019313R1, 019313R2, and their respective mutagenized parent strains used to initiate drug selection, WT1 and WT2, were subjected to whole-genome sequencing. Comparison of the resistant and parent genome sequences identified a single nucleotide variant (SNV) which was present in 100% of reads in 019313R1 and 63% of reads in 019313R2 but not present in either susceptible parent genomes (Table 1). No other SNV were detected at >40% prevalence in either resistant populations relative to the corresponding parent populations. The identified SNV was a T-to-A mutation in the gene PF3D7_1128400 characterized as a bifunctional FPPS/GGPPS and resulted in a Ser228-to-Thr change in the protein (Figure 2B; 2, 4). IPP is a known substrate of the FPPS/GGPPS, and in the primary sequence Ser228 is adjacent to conserved KT residues and an Asp-rich region required for catalysis in all homologous FPPS and GGPPS enzymes (Figure 2C). *Pf*FPPS/GGPPS was a strong candidate for further validation as the molecular target of MMV019313.

Overexpression and an S228T variant of *Pf*FPPS/GGPPS confers resistance to MMV019313

We determined whether overexpression of wildtype *Pf*FPPS/GGPPS was sufficient to confer resistance to MMV019313. A transgene encoding FPPS/GGPPS-GFP under the control of either the ribosomal L2 protein (*RL2*; PF3D7_1132700) or calmodulin (*CaM*; PF3D7_1434200) promoter was integrated into an engineered *att*B locus in $Dd2^{attb}$ parasites (28). Expression of the CaM promoter is 10 to 50-fold greater across the life cycle than that of the RL2 promoter based on RNA-seq data, resulting in appreciably greater FPPS/GGPPS-GFP protein (Figure S3A; 29). Therefore, we compared the effect of no, moderate (RL2), and high (CaM) levels of FPPS/GGPPS-GFP overexpression on susceptibility to MMV019313. As shown in Figure 3A, overexpression of FPPS/GGPPS-GFP results in a dose-dependent increase in the EC_{50} of MMV019313 with intermediate-level resistance to MMV019313 observed in the RL2-FPPS/GGPPS-GFP strain and high-level resistance observed in the CaM-FPPS/GGPPS-GFP strain. Notably growth inhibition by MMV019313 in the CaM-FPPS/GGPPS-GFP strain could no longer be rescued by IPP, indicating that complete resistance to inhibition of the specific IPP-rescuable target had been achieved (Figure S3B).

We also determined whether the S228T variant of GGPPS confers MMV019313 resistance. Initially we attempted to introduce the S228T mutation into the *fpps/ggpps* gene in the *P. falciparum* genome using CRISPR-Cas9 mutagenesis but were unable to recover mutant parasites. As an alternative, we overexpressed the FPPS/GGPPS(S228T)-GFP variant using the "moderate" RL2 promoter and compared its effect on MMV019313 susceptibility with that of the wild-type RL2-FPPS/GGPPS-GFP. Overexpression of the FPPS/GGPPS(S228T)-GFP variant, even at moderate levels, caused an 18-fold increase in the EC_{50} which did not increase further with IPP rescue, indicating that complete resistance to inhibition of the specific, IPP-rescuable target had been achieved (Figure 3B and S3C). Because moderate overexpression of the S228T variant caused greater MMV019313 resistance than moderate overexpression of wildtype *Pf*FPPS/GGPPS, we conclude that the S228T variant is sufficient to confer resistance independent of overexpression. Altogether these results clearly demonstrated that the mechanism-of-action of MMV0193313 is dependent on *Pf*FPPS/GGPPS.

MMV019313 specifically inhibits the enzymatic activity of *Pf*FPPS/GGPPS

To confirm that *Pf*FPPS/GGPPS is the molecular target of MMV019313, we directly measured MMV019313 inhibition in enzymatic assays. Consistent with a previous report, purified *Pf*FPPS/GGPPS catalyzed the production of both farnesyl(C15)-PP and geranylgeranyl(C20)-PP (2). To measure the inhibitory effect of MMV019313, we determined its IC_{50} for FPP and GGPP production in two conditions. In the first "non-saturating" condition, substrate concentrations equaled K_M values (Figure S4), the concentration at which the rate of reaction is half-maximal. In the second "k_{cat}" condition, substrate concentrations were saturating and the rate of reaction was maximal. Measuring inhibitor effects in both "non-saturating" and "k_{cat}" conditions increases the sensitivity for detecting different types of inhibitors (competitive, non-competitive, uncompetitive). We found the IC_{50} value was 330 nM for FPP production under "non-saturating" conditions, comparable to its EC_{50} value in cellular growth inhibition assays (Figure 1B and S5). MMV019313 was identified by its IPP rescue phenotype in cell growth assays wherein addition of exogenous substrate increases enzymatic rates, indicating that physiological conditions are likely sub-saturating. Therefore its IC_{50} value measured in sub-saturating condition is more relevant for comparison to its EC_{50} value for growth inhibition. Under "k_{cat}" conditions, IC_{50} values were 2.0 μM for FPP production and 9.8 μM for GGPP production (Figure 4A-B).

Since inhibition was detectable in both conditions, assays of mutant and human enzymes were performed at saturating conditions which gives higher signal-to-noise. Significantly MMV019313 at concentrations up to 200 μM did not inhibit human FPPS or GGPPS activity, indicating that it was at least 100-fold selective for *Pf*FPPS/GGPPS over human homologs (Figure 4A-B). In contrast, the most selective bisphosphonate identified by a previous study, BPH-703, showed only a 2.6-fold selectivity for *Pf*FPPS/GGPPS versus human FPPS and 3.6-fold selectivity versus human GGPPS in enzymatic assays (Figure 4C-D; 6).

MMV019313 binds a novel site on *Pf*FPPS/GGPPS, distinct from that of bisphosphonates

The lack of inhibition of human FPPS and GGPPS by MMV019313 was intriguing since *Pf*FPPS/GGPPS is structurally related to human FPPS and GGPPS and all are inhibited by bisphosphonates (6). Co-crystal structures have shown that bisphosphonates, zoledronate and its lipophilic analog BPH-703, bind in the allylic substrate (DMAPP, GPP, or FPP) site in the *Plasmodium vivax* FPPS/GGPPS homolog (6). This binding is similar to what is observed in

bisphosphonate-mammalian FPPS complexes (30-33). To determine whether MMV019313 and bisphosphonates share a common binding site, we compared the effect of the S228T variant on inhibition by MMV019313 and the bisphosphonate BPH-703. MMV019313 and BPH-703 both inhibited wild-type *Pf*FPPS/GGPPS activity. However only MMV019313 inhibition was decreased by over 10-fold in the S228T variant (Figure 4A-D). This difference in their *in vitro* enzyme inhibition was consistent with the effect on parasite growth inhibition, in which moderate overexpression of the S228T variant conferred resistance to MMV019313 but not BPH-703 (Figure S5). In addition, residue S228 is adjacent to the IPP binding site in the bisphosphonate-PvFPPS/GGPPS structures and distal from the bound bisphosphonate. These results demonstrate that MMV019313 has a novel binding mode, distinct from the known allylic substrate site occupied by bisphosphonates, one which may confer its specificity for *Plasmodium* FPPS/GGPPS over human homologs.

Because our biochemical results indicated that MM019313 binds a new site which is unique to *Pf*FPPS/GGPPS, we performed molecular docking calculations to evaluate the likelihood of MMV019313 binding at known small molecule binding sites in *Pf*FPPS/GGPPS. Three small molecule binding sites have been identified in FPPS and GPPS enzymes: 1) the allylic substrate binding site, which is also occupied by bisphosphonates, 2) the IPP binding site, and 3) an allosteric site identified in *Hs*FPPS (34). Because both the allylic substrate and IPP sites have been structurally characterized in *Pv*FPPS/GGPPS, we used the rigid body docking program Glide to generate poses with MMV019313 bound to these sites and estimate the binding free energy of each pose (35-37). The binding affinity estimated for the MMV019313 poses were $>10^8$ weaker than bisphosphonate at the allylic site and $>10^5$ weaker than IPP at its site (Table S2). Therefore, the modeling suggests that MMV019313 is unlikely to bind either the allylic substrate or IPP site. We also attempted to dock MMV019313 into other potential binding pockets in the *Pv*FPPS/GGPPS apo structure but with inconclusive results.

Discussion

Farnesyl and geranylgeranyl diphosphate synthase (FPPS and GGPPS) are key branch point enzymes in isoprenoid biosynthesis. Human cells contain separate FPPS and GGPPS enzymes. An important class of clinical drugs, nitrogen-containing bisphosphonates, inhibits human FPPS in osteoclasts and block their function and proliferation (31). Because osteoclasts are responsible for bone resorption, bisphosphonates are highly effective for treatment of osteoporosis and other bone remodeling diseases. Bisphosphonates are chemically stable analogs of inorganic pyrophosphate containing a P-C-P bond in place of the phosphodiester, which accounts for both its inhibition of FPPS (acting as an analog of the allylic diphosphate substrate) and its high selectivity for osteoclasts (depositing in bone mineral which is composed of calcium and phosphate). Unfortunately the charge state of bisphosphonates is a major liability in other therapeutic applications, as they are poorly bioavailable, rapidly cleared by the kidney, and do not achieve therapeutic levels in serum for treatment of non-bone diseases (5, 8, 25, 38).

*Pf*FPPS/GGPPS, the molecular target of MMV019313 as demonstrated in this study, closely resembles mammalian FPPS enzymes in sequence, structure, and inhibition by bisphosphonates (2, 6). Like human FPPS, it is a central node in cellular isoprenoid biosynthesis vulnerable to drug inhibition (4, 31, 39). In *Plasmodium*, FPP and GGPP are required for the biosynthesis of prenylated proteins, the prenyl modification of ubiquinone, and other isoprenoid products, such that inhibition of *Pf*FPPS/GGPPS disrupts multiple cellular pathways (3, 40-43). Previously lipophilic bisphosphonates modified with an alkyl chain to increase their cell

permeability were shown to inhibit *Pv*FPPS/GGPPS homolog and clear both blood- and liver-stage *Plasmodium* parasites in mice infection models (5, 6). Importantly, these results validated *Plasmodium* FPPS/GGPPS as an antiparasitic drug target for both acute malaria treatment and malaria chemoprophylaxis.

Our identification of MMV019313 further addresses two key hurdles in the development of *Pf*FPPS/GGPPS inhibitors as antimalarial drugs. First, MMV019313 represents the first non-bisphosphonate class of *Plasmodium* FPPS/GGPPS inhibitors with superior physicochemical properties. Many efforts have been made to develop modified bisphosphonates or non-bisphosphonate compounds as FPPS and/or GGPPS inhibitors for treatment of soft-tissue cancers and infectious diseases (34, 44-47). Unlike bisphosphonates, MMV019313 has drug-like physicochemical properties satisfying the Rule of 5 and does not need to mimic a charged diphosphate substrate to achieve FPPS/GGPPS inhibition (25). As a compound in the Malaria Box library, it has already been tested in a panel of bioactivity and pharmacokinetic assays with encouraging results (25). Furthermore the results of >300 assays characterizing Malaria Box compounds as part of an innovative "open source" drug discovery effort by many groups will be a rich source of information (25, 48-50).

Second, MMV019313 has high selectivity for *Pf*FPPS/GGPPS over human FPPS and GGPPS, minimizing the potential for mechanism-based (e.g. "on-target") toxicity. In fact, we could not detect any inhibition of human FPPS or GGPPS indicating selectivity at the enzymatic level of at least 100-fold. Consistent with this lack of enzymatic inhibition, MMV019313 showed no cytotoxity against a panel of 60 human cancer cell lines at 10 μM (25). In contrast, the most selective bisphosphonate BPH-703 identified by No *et al* showed 2.6-3.6-fold selectivity in our enzymatic assays (corresponding to a reported therapeutic index of 193 in growth inhibition assays; 6). Our results suggest that MMV019313 binds a novel site in *Pf*FPPS/GGPPS that is either absent from or substantially different in the human homologs, which may explain its high selectivity. Altogether MMV019313 offers a distinct and promising starting point for development of antimalarial FPPS/GGPPS inhibitors, which circumvents the inherent liabilities of the bisphosphonate pharmacophore and greatly improves on their selectivity.

Our immediate priority is to obtain structures of the inhibitor-enzyme complex to aid in structure-based design of MMV019313 derivatives with higher potency, as well as discovery of additional chemical scaffolds that occupy this new binding site. A potential challenge is that the FPPS structure is dynamic during catalysis. For example, the human FPPS is known to undergo at least two critical conformational changes (31): The first is from an "open" apo form to a "closed" conformation upon binding of the allylic substrate, which is associated with drastically increased affinity for the allylic substrate (and bisphosphonates that mimic this substrate) as well as orders the IPP binding pocket. The second structural change occurs upon IPP binding and sequesters the active site from bulk solvent. Several attempts to obtain co-crystal structures of MMV019313 with *Pv*FPPS/GGPPS under conditions in which bisphosphonate-*Pv*FPPS/GGPPS crystals were obtained (presumed to correspond to the "closed" conformation) have been unsuccessful (personal communication, Dr. Raymond Hui). Additional crystallization conditions may require testing in the presence and absence of different allylic substrates and IPP, as their binding could affect the binding of MMV019313. Given the dynamic and complex mechanism of FPPS and GGPPS enzymes, detailed kinetic characterization of MMV019313 inhibition will be important to complement structural studies.

Since the S228T variant distinguishes between MMV019313 and bisphosphonate binding to *Pf*FPPS/GGPPS, obtaining its structure to compare with wildtype FPPS/GGPPS will also offer clues to this new mode-of-inhibition. The resistance caused by the S228T variant could be explained by a direct contact between Ser228 and MMV019313 in a new small molecule binding pocket. But because the change from Ser to Thr is quite conservative, the addition of a methyl group, it seems more likely that Ser228 is involved in conformational dynamics important for catalysis. Structural analysis of this variant enzyme may reveal altered conformational states underlying the resistance to MMV019313.

Optimization of the bioactivity and pharmacokinetic properties of MMV019313 derivatives will be priorities for their development as antimalarials. The luciferase-based enzymatic assays performed in our study are robust for detection of effective inhibitors and can be adapted to high-throughput screening of small molecule libraries (in contrast we found a commercially-available colorimetric assay was not sufficiently sensitive; 51). Inhibitor-enzyme structures will greatly accelerate optimization for potency against the *Plasmodium* FPPS/GGPPS, while simultaneously minimizing binding to the human homologs. *P. falciparum* strains overexpressing wildtype or the S228T variant, generated during this study, can also be re-tooled as secondary cellular assays for on-target specificity. The drug properties of MMV019313 derivatives will be optimized in standard absorption-distribution-metabolism-excretion-toxicity (ADME-T) assays. For example, we found that while MMV019313 is stable to human liver microsomal enzymes ($t_{½}$> 159 min), its $t_{½}$ in mouse liver microsomes was 4 min. This metabolic instability may account for a <1μM peak serum concentration following oral administration in mice and will need to be addressed before derivatives can be tested in mouse models of *Plasmodium* infection (25).

Finally, our study demonstrates two methodological improvements. First, we took advantage of a quantitative screen for IPP chemical rescue using a range of inhibitor concentrations, rather than a single high dose. The increased sensitivity allowed us to identify MMV019313, though it was missed in prior screens. It also permits the screen to be performed with geranylgeraniol, which is significantly less costly than IPP, since so far all identified inhibitors that rescue with IPP also show at least a partial rescue of parasite growth inhibition with geranylgeraniol (24, 52). Second, we employed chemical mutagenesis to select for drug-resistant mutants, which has not previously been reported in *Plasmodium* to our knowledge but has been used for genetic screens in *Toxoplasma gondii* (27). Notably we were unable to select MMV019313-resistant parasites in the absence of chemical mutagenesis, though this same protocol was effective in selecting drug resistance against MMV008138 when performed in parallel (23). Our experience suggests that the use of chemical mutagens will increase successful selection for drug resistance in *Plasmodium* parasites, which is the most common method employed to identify drug targets from phenotypic drug screens (18-20). The low frequency of *in vitro* MMV019313 resistance also indicates that clinical resistance will also be less frequent to MMV019313 and its derivatives.

Methods

***P. falciparum in vitro* cultures.** *Plasmodium falciparum* W2 (MRA-157) and Dd2^{attB} (MRA-843) were obtained from MR4. Parasites were grown in human erythrocytes (2% hematocrit) in RPMI 1640 media supplemented with 0.25% Albumax II (GIBCO Life

Technologies), 2 g/L sodium bicarbonate, 0.1 mM hypoxanthine, 25 mM HEPES (pH 7.4), and 50 µg/L gentamycin, at 37°C, 5% O_2, and 5% CO_2. For passage of drug-treated, IPP-rescued parasites, the media was supplemented with 5 µM drug and 200 µM IPP (Isoprenoids LC or NuChem). For comparison of growth between different treatment conditions, cultures were carried simultaneously and handled identically with respect to media changes and addition of blood cells

Chemical handling. Malaria Box compounds were received as 10 mM DMSO stocks in 96-well plates and diluted three-fold manually in DMSO. Fosmidomycin was included in control wells. Two-fold serial dilutions of the 96-well plates were performed on Velocity11. Compound stocks stored in DMSO were diluted for growth assays. MMV019313 was purchased from ChemDiv

qHTS screen for IPP chemical rescue. Growth assays were performed in 384-well clear bottom assay plates (E and K scientific, Santa Clara, CA). Drug (100-400 nL) was added directly to each well using PinTool (V&P Scientific) on a Sciclone ALH3000 (Caliper Sciences). Using the Titertek Multidrop 384, first 40 µL of growth media with and without 375 µM IPP was dispensed, followed by 10 µL ring-stage *P. falciparum* D10 parasites (parasitemia 0.8% in 10% hematocrit) into 384-well plates using the Titertek Multidrop 384. The final assay consisted of 50 µL ring-stage cultures at 0.8% parasitemia/ 2% hematocrit and drug concentrations from 0.01-26.7 µM ± 300 µM IPP. The plate was incubated at 37°C for 72 h. Parasites were lysed with 10 µL 5mM EDTA, 1.6% Triton-X, 20mM Tris-HCl and 0.16% Saponin containing 0.1% Sybr Green I (Invitrogen). The plates were then incubated at -80 °C for 20 min and thawed at room temperature overnight in the dark. Fluorescence was detected using Flexstation II- 384. Compounds that showed IPP rescue of growth inhibition at 1 or more drug concentrations in the initial 384-well high-throughput screen were re-tested in a 96-well growth assay.

Growth inhibition assays to determine EC_{50} values. *P. falciparum* cultures (125 µL) were grown in 96-well plates containing serial dilution of drugs in triplicate. Media was supplemented with 200 µM IPP as indicated. Growth was initiated with ring-stage parasites at 1% parasitemia and 0.5% hematocrit. Plates were incubated for 72h. Growth was terminated by fixation with 1% formaldehyde and parasitized cells were stained with 50 nM YOYO-1 (Invitrogen). Parasitemia was determined by flow cytometry. Data were analyzed by BD C6 Accuri C-Sampler software, and EC_{50} curves plotted by GraphPad Prism.

***P. falciparum* mutagenesis and resistance selection.** Late-stage parasites were purified using a SuperMACS II separator (Miltenyi Biotec) and incubated in complete medium with 8.3 – 2025 µM ethyl methanesulfonate (EMS, 6 concentrations total) for 2 hours. The concentrations of EMS used were selected by determining the EC_{50} in 72h parasite growth inhibition assays. The highest concentration used for mutagenesis was equal to the EC_{50} in order to maximize the selection pressure. The mutagen was then serially diluted 1:3 to test lower concentrations that might give lower mutation rates and therefore a lower frequency of passenger mutations. Mutagenized parasites were washed and separated into wells of 10 mL total volume (approximately 10% parasitemia, 2 % HCT). MMV019313 drug selection was applied to one well for each mutagenesis condition at 600 nM (approximately EC_{75}), while the other well was left untreated in order to serve as a control for whole genome sequencing. Parasites were fed

daily for the first week and every 3 days thereafter. Each culture was split in half every 6 days in order to introduce fresh RBC. Drug pressure was maintained for 32 days, with no observable parasite growth. After 32 days of selection, half of the culture from each EMS condition was removed from drug pressure. In these cultures, parasites which showed resistance to MMV019313 by a standard drug assay were observable after 7 days at all EMS conditions used. The parasites treated with the two lowest concentrations of EMS were selected for whole genome sequencing.

Whole Genome Sequencing. *Plasmodium falciparum* strains were sequenced by Illumina sequencing as described previously (53). Briefly, NEBNext DNA library reagents (NEB) and NEXTflex DNA barcode adapters (Bioo Scientific) were used to prepare PCR-free libraries (54). Eight whole genome gDNA libraries were multiplexed and spiked with 8% PhiX control. Single-end sequencing was performed across two lanes on an Illumina HiSeq 2500 system. Data was analyzed using tools available in the Galaxy platform (55-57). Sequencing reads were mapped against the *P. falciparum* 3D7v.10.0 reference genome using the Burrows-Wheeler Alignment tool (58). Sequencing data was visualized using Integrative Genomics Viewer (IGV) (59, 60). Variants were called using Freebayes (61) and filtered for Quality >100 and Read Depth >30 using GATK tools (62). SnpEff was used to annotate the list of variants based on the *P. falciparum* 3D7v9.1 reference genome (63). Sequencing data have been deposited to the SRA.

***P. falciparum* Transfections.** An *E. coli* codon optimized version of *Pf*FPPS/GGPPS (PF3D7_1128400) was designed and synthesized by GeneWiz. Quick change mutagenesis was used to mutate GGPPS serine 228 to a threonine in the pUC vector provided by GeneWiz. These constructs were then moved into the pLN transfection plasmid designed for Bxb1 mycobacteriophage integrase system (64). The In-fusion cloning kit (Clontech) was used for all cloning. Restriction enzymes *Avr*II and *Bsi*WI were used to linearize the pLN vector. GGPPS was designed to have a *C*-terminal GFP tag. All transgenes were driven with either the ribosomal L2 protein (RL2) promoter (PF3D7_1132700) or the calmodulin (CaM) promoter (PF3D7_1434200) as denoted.

Transfections were carried out as previously described (65). Briefly, 400 µL fresh red blood cells were preloaded with 100 µg of both pINT, which carries the bacteriophage integrase, and pRL2, which carries the gene of interest and the blasticidin resistance cassette, using a BioRad Gene-Pulser Xcell Electroporator. Electroporation conditions were infinite resistance, 310 V, and 950 µF using a 2 mm cuvette. Preloaded red blood cells were combined with 2.5 mL ~20% schizont Dd2^{attB} parasites and allowed to recover for 2 days before selection pressure was applied. Transfected parasites were selected with 2.5 µg/mL blasticidin are were detectable by thin smear within 15 days. Integration was confirmed by PCR and identity of the transgene was confirmed by sanger sequencing.

Immunoblots. Parasites expressing either ACP_L-GFP or one of the FPPS/GGPPS constructs generated in this study were isolated by saponin lysis and resuspended in 1xNuPage LDS sample buffer (Invitrogen). Whole cell lysate was separated by SDS-PAGE using 4-12% Bis-Tris gels (Initrogen) and transferred to nitrocellulose using a Trans Turbo-blot (BioRad). Membranes were blocked with 3% BSA, probed with 1:5,000 monoclonal anti-GFP JL-8

(BioRad) overnight, washed, then probed with 1:10,000 IRDye 680LT goat-anti-mouse. The Western was imaged using a Oddysey Imager (LiCor Biosciences).

Live microscopy. Infected red blood cells were treated with Hoescht to stain the nucleus. Single z-stack images were collected on an epifluorescence Nikon eclipse.

Quantative PCR. Quantitative PCR was performed as previously published(21). Briefly, parasites from 200 µL of culture were isolated by saponin lysis followed by PBS wash to remove extracellular DNA. DNA was purified using DNeasy Blood and Tissue kit (Qiagen). Primers were designed to target genes found on the apicoplast or nuclear genome: *tufA* (apicoplast) 5′-GATATTGATTCAGCTCCAGAAGAAA-3′ / 5′-ATATCCATTTGTGTGGCTCCTATAA-3′ and *CHT1* (nuclear) 5′-TGTTTCCTTCAACCCCTTTT-3′ / 5′-TGTTTCCTTCAACCCCTTTT-3′. Reactions contained template DNA, 0.15 µM of each primer, and 0.75× LightCycler 480 SYBR Green I Master mix (Roche). PCR reactions were performed at 56°C primer annealing and 65°C template extension for 35 cycles on a Lightcycler 6500 (Roche). For each time point, the apicoplast∶nuclear genome ratio of the fosmidomycin-treated positive control, chloramphenicol-treated negative control, or MMV019313-treated experiment were calculated relative to that of an untreated control collected at the same time.

Recombinant protein purification. Full length constructs of *Pf*FPPS/GGPPS, *Hs*FPPS, and *Hs*GGPPS were cloned into pET28a with an n-terminal hexahistidine tag. The *P. falciparum* FPPS/GGPPS was codon optimized for expression in *E. coli* (GeneWiz). *Pf*FPPS/GGPPS was mutagenized (S228T) using quick change mutagenesis. When expressed in *E. coli,* *Pf*FPPS/GGPPS (wt and S228T) and *Hs*FPPS were toxic. Cultures were supplemented with 0.4% glucose and grown to OD_{600} of 0.8-1 and induced with 0.5 mM IPTG. *Hs*GGPPS was grown without supplementation to an OD_{600} of 0.8-1. All cultures were induced for 4 hours at 37 °C, then harvested. Cells were lysed in 20 mM HEPES pH 8.0, 150 mM NaCl, 2 mM $MgCl_2$, and protease inhibitor cocktail using sonication. Cleared lysates were either mixed with Talon metal affinity resin (Clonetech) or purified over 5 ml HisTrap columns (GE Healthcare). His tagged protein was purified with a single step purification eluting with buffer with 300 mM imidazole. Proteins were dialyzed to remove imidazole and flash frozen.

***In vitro* FPPS/GGPPS assays.** FPPS/GGPPS activity was measured by monitoring pyrophosphate release using the Lonza PPiLight kit under kinetic conditions. Drug and either 20 µg/ml *Pf*FPPS/GGPPS, 40 µg/ml *Hs*GGPPS, or 100 µg/ml *Hs*FPPS protein were incubated for 30 min room temperature. The reaction was initiated by the addition of Lonza PPiLight kit reaction mix and substrates. Saturating substrate conditions were 100 µM GPP or FPP, and 200 µM IPP. Sub-saturation conditions were K_M conditions as shown in Figure S4. Luciferase activity was monitored overtime using a BioTeck plate reader.

MMV019313 ligand docking. Using a solved *Pv*FPPS/GGPPS structure (PDB: 3EZ3, zoledronate and IPP bound) as a receptor model protein preparation wizard was used to add back in missing hydrogens and side chains. All crystallographic waters were removed. Hydrogen bonds were calculated using Epik at pH 8 (±1). The protein structure was minimized using OPL3 force field. MMV019313 was docked using glide to receptor grids generated from the relevant crystallized small molecules.

Acknowledgements

We are grateful to Medicines for Malaria Ventures (MMV) for providing the Malaria Box compounds and making this valuable library freely available, as well as GlaxoSmithKline for their screening efforts that first identified MMV019313 (TCMDC-123889). We would like to thank Dr. Susmitha Suresh for performing drug screens and Dr. Felice Kelly for advice on how to chemically mutagenize our parasites for resistance selection. We are grateful to Dr. James Dunford (University of Oxford) for advice in developing the *in vitro* enzyme activity assays. We also would like to acknowledge Dr. Wei Zhu and Professor Eric Oldfield (University of Illinois, Urbana-Champaign) for *in vitro P. vivax* GGPPS activity assays and providing BPH-703.

Financial Disclosure

Funding support for this project was provided by the Stanford Consortium for Innovation, Design, Evaluation and Action (C-IDEA), NIH 1K08AI097239 (EY), NIH 1DP5OD012119 (EY), the Burroughs Wellcome Fund Career Award for Medical Scientists (EY), the Burroughs Wellcome Fund Investigators in Pathogenesis of Infectious Disease (PATH) Award (ML), and the Stanford School of Medicine Dean's Postdoctoral Fellowship (JEG).

References

1. Jomaa H, et al. (1999) Inhibitors of the nonmevalonate pathway of isoprenoid biosynthesis as antimalarial drugs. *Science* 285(5433):1573–1576.

2. Jordão FM, et al. (2013) Cloning and characterization of bifunctional enzyme farnesyl diphosphate/geranylgeranyl diphosphate synthase from *Plasmodium falciparum*. *Malar J* 12(1):184.

3. Tonhosolo R, et al. (2005) Identification, molecular cloning and functional characterization of an octaprenyl pyrophosphate synthase in intra-erythrocytic stages of *Plasmodium falciparum*. *Biochem J* 392(Pt 1):117–126.

4. Artz JD, et al. (2011) Molecular characterization of a novel geranylgeranyl pyrophosphate synthase from *Plasmodium* parasites. *J Biol Chem* 286(5):3315–3322.

5. Singh AP, et al. (2010) Lipophilic bisphosphonates are potent inhibitors of *Plasmodium* liver-stage growth. *Antimicrob Agents Chemother* 54(7):2987–2993.

6. No JH, et al. (2012) Lipophilic analogs of zoledronate and risedronate inhibit *Plasmodium* geranylgeranyl diphosphate synthase (GGPPS) and exhibit potent antimalarial activity. *Proc Natl Acad Sci USA* 109(11):4058–4063.

7. Michael B Martin, et al. (2001) Bisphosphonates Inhibit the Growth of *Trypanosoma brucei, Trypanosoma cruzi, Leishmania donovani, Toxoplasma gondii,* and *Plasmodium falciparum*: A Potential Route to Chemotherapy. *J Med Chem* 44(6):909–916.

8. Jordão FM, et al. (2011) In vitro and in vivo antiplasmodial activities of risedronate and its interference with protein prenylation in *Plasmodium falciparum*. *Antimicrob Agents Chemother* 55(5):2026–2031.

9. Ghosh S, et al. (2004) Effects of bisphosphonates on the growth of *Entamoeba histolytica* and *Plasmodium* species in vitro and in vivo. *J Med Chem* 47(1):175–187.

10. Nallan L, et al. (2005) Protein farnesyltransferase inhibitors exhibit potent antimalarial activity. *J Med Chem* 48(11):3704–3713.

11. Eastman RT, et al. (2007) Resistance mutations at the lipid substrate binding site of *Plasmodium falciparum* protein farnesyltransferase. *Mol Biochem Parasitol* 152(1):66–71.

12. Eastman RT, et al. (2005) Resistance to a protein farnesyltransferase inhibitor in *Plasmodium falciparum*. *J Biol Chem* 280(14):13554–13559.

13. Fernandes JF, et al. (2015) Fosmidomycin as an antimalarial drug: a meta-analysis of clinical trials. *Future Microbiol* 10(8):1375–1390.

14. Sinigaglia L, Varenna M, Casari S (2007) Pharmacokinetic profile of bisphosphonates in the treatment of metabolic bone disorders. *Clin Cases Miner Bone Metab* 4(1):30–36.

15. Van Voorhis WC, et al. (2007) Efficacy, pharmacokinetics, and metabolism of tetrahydroquinoline inhibitors of *Plasmodium falciparum* protein farnesyltransferase. *Antimicrob Agents Chemother* 51(10):3659–3671.

16. Tsuchiya T, et al. (1982) Pharmacokinetics and metabolism of fosmidomycin, a new phosphonic acid, in rats and dogs. *Eur J Drug Metab Pharmacokinet* 7(1):59–64.

17. Spangenberg T, et al. (2013) The open access malaria box: a drug discovery catalyst for neglected diseases. *PLoS ONE* 8(6):e62906.

18. Rottmann M, et al. (2010) Spiroindolones, a potent compound class for the treatment of malaria. *Science* 329(5996):1175–1180.

19. Gamo FJ, et al. (2010) Thousands of chemical starting points for antimalarial lead identification. *Nature* 465(7296):305–310.

20. Guiguemde WA, et al. (2010) Chemical genetics of *Plasmodium falciparum*. *Nature* 465(7296):311–315.

21. Yeh E, Derisi JL (2011) Chemical rescue of malaria parasites lacking an apicoplast defines organelle function in blood-stage *Plasmodium falciparum*. *PLoS Biol* 9(8):e1001138.

22. Bowman JD, et al. (2014) Antiapicoplast and gametocytocidal screening to identify the mechanisms of action of compounds within the malaria box. *Antimicrob Agents Chemother* 58(2):811–819.

595 23. Wu W, et al. (2015) A chemical rescue screen identifies a *Plasmodium falciparum*
596 apicoplast inhibitor targeting MEP isoprenoid precursor biosynthesis. *Antimicrob Agents*
597 *Chemother* 59(1):356–364.

598 24. DeRisi JL, et al. (2014) *UCSF DeRisi Lab MMV Box Apicoplast Screening* (EMBL-EBI)
599 doi:10.6019/CHEMBL2448809.

600 25. Van Voorhis WC, et al. (2016) Open Source Drug Discovery with the Malaria Box
601 Compound Collection for Neglected Diseases and Beyond. *PLoS Pathog* 12(7):e1005763.

602 26. Amberg-Johnson K, Ganesan SM, Lorenzi HA, Niles JC, Yeh E (2017) A first-in-class
603 inhibitor of parasite FtsH disrupts plastid biogenesis in human pathogens. *bioRxiv*:108910.

604 27. Franco M, et al. (2016) A Novel Secreted Protein, MYR1, Is Central to Toxoplasma's
605 Manipulation of Host Cells. *MBio* 7(1):e02231–15.

606 28. Nkrumah LJ, et al. (2006) Efficient site-specific integration in *Plasmodium falciparum*
607 chromosomes mediated by mycobacteriophage Bxb1 integrase. *Nat Methods* 3(8):615–
608 621.

609 29. Otto TD, et al. (2010) New insights into the blood-stage transcriptome of *Plasmodium*
610 *falciparum* using RNA-Seq. *Mol Microbiol* 76(1):12–24.

611 30. Rondeau J-M, et al. (2006) Structural Basis for the Exceptional in vivo Efficacy of
612 Bisphosphonate Drugs. *ChemMedChem* 1(2):267–273.

613 31. Kavanagh KL, et al. (2006) The molecular mechanism of nitrogen-containing
614 bisphosphonates as antiosteoporosis drugs. *Proc Natl Acad Sci USA* 103(20):7829–7834.

615 32. Zhang Y, et al. (2013) Chemo-Immunotherapeutic Anti-Malarials Targeting Isoprenoid
616 Biosynthesis. *ACS Med Chem Lett* 4(4):423–427.

617 33. Yokoyama T, et al. (2015) Protonation State and Hydration of Bisphosphonate Bound to
618 Farnesyl Pyrophosphate Synthase. *J Med Chem* 58(18):7549–7556.

619 34. Jahnke W, et al. (2010) Allosteric non-bisphosphonate FPPS inhibitors identified by
620 fragment-based discovery. *Nat Chem Biol* 6(9):660–666.

621 35. Halgren TA, et al. (2004) Glide: a new approach for rapid, accurate docking and scoring.
622 2. Enrichment factors in database screening. *J Med Chem* 47(7):1750–1759.

623 36. Friesner RA, et al. (2004) Glide: a new approach for rapid, accurate docking and scoring.
624 1. Method and assessment of docking accuracy. *J Med Chem* 47(7):1739–1749.

625 37. Friesner RA, et al. (2006) Extra precision glide: docking and scoring incorporating a
626 model of hydrophobic enclosure for protein-ligand complexes. *J Med Chem* 49(21):6177–
627 6196.

628 38. Cremers SCLM, Pillai G, Papapoulos SE (2005) Pharmacokinetics/pharmacodynamics of
629 bisphosphonates: use for optimisation of intermittent therapy for osteoporosis. *Clin*
630 *Pharmacokinet* 44(6):551–570.

631 39. Luckman SP, et al. (1998) Nitrogen-containing bisphosphonates inhibit the mevalonate
632 pathway and prevent post-translational prenylation of GTP-binding proteins, including
633 Ras. *J Bone Miner Res* 13(4):581–589.

634 40. de Macedo CS, Uhrig ML, Kimura EA, Katzin AM (2002) Characterization of the
635 isoprenoid chain of coenzyme Q in *Plasmodium falciparum*. *FEMS Microbiol Lett*
636 207(1):13–20.

637 41. Tonhosolo R, et al. (2009) Carotenoid biosynthesis in intraerythrocytic stages of
638 *Plasmodium falciparum*. *J Biol Chem* 284(15):9974–9985.

639 42. Gabriel HB, et al. (2015) Squalestatin is an inhibitor of carotenoid biosynthesis in
640 *Plasmodium falciparum*. *Antimicrob Agents Chemother* 59(6):3180–3188.

641 43. Chakrabarti D, et al. (2002) Protein farnesyltransferase and protein prenylation in
642 *Plasmodium falciparum*. *J Biol Chem*. doi:10.1074/jbc.M202860200.

643 44. Chen S-H, Lin S-W, Lin S-R, Liang P-H, Yang J-M (2013) Moiety-linkage map reveals
644 selective nonbisphosphonate inhibitors of human geranylgeranyl diphosphate synthase. *J*
645 *Chem Inf Model* 53(9):2299–2311.

646 45. Liu J, et al. (2014) Syntheses and characterization of non-bisphosphonate quinoline
647 derivatives as new FPPS inhibitors. *Biochim Biophys Acta* 1840(3):1051–1062.

648 46. Marzinzik AL, et al. (2015) Discovery of Novel Allosteric Non-Bisphosphonate Inhibitors
649 of Farnesyl Pyrophosphate Synthase by Integrated Lead Finding. *ChemMedChem*
650 10(11):1884–1891.

651 47. Zhang Y, et al. (2009) Lipophilic bisphosphonates as dual farnesyl/geranylgeranyl
652 diphosphate synthase inhibitors: an X-ray and NMR investigation. *J Am Chem Soc*
653 131(14):5153–5162.

654 48. Ullah I, Sharma R, Biagini GA, Horrocks P (2017) A validated bioluminescence-based
655 assay for the rapid determination of the initial rate of kill for discovery antimalarials. *J*
656 *Antimicrob Chemother* 72(3):717–726.

657 49. Allman EL, Painter HJ, Samra J, Carrasquilla M, Llinás M (2016) Metabolomic Profiling
658 of the Malaria Box Reveals Antimalarial Target Pathways. *Antimicrob Agents Chemother*
659 60(11):6635–6649.

660 50. Paul AS, Moreira CK, Elsworth B, Allred DR, Duraisingh MT (2016) Extensive Shared
661 Chemosensitivity between Malaria and Babesiosis Blood-Stage Parasites. *Antimicrob*
662 *Agents Chemother* 60(8):5059–5063.

663 51. Crowther GJ, et al. (2011) Identification of inhibitors for putative malaria drug targets
664 among novel antimalarial compounds. *Mol Biochem Parasitol* 175(1):21–29.

665 52. Zhang B, et al. (2011) A second target of the antimalarial and antibacterial agent
666 fosmidomycin revealed by cellular metabolic profiling. *Biochemistry* 50(17):3570–3577.

667 53. Straimer J, et al. (2012) Site-specific genome editing in *Plasmodium falciparum* using
668 engineered zinc-finger nucleases. *Nat Methods* 9(10):993–998.

669 54. Kozarewa I, et al. (2009) Amplification-free Illumina sequencing-library preparation
670 facilitates improved mapping and assembly of (G+C)-biased genomes. *Nat Methods*
671 6(4):291–295.

672 55. Giardine B, et al. (2005) Galaxy: a platform for interactive large-scale genome analysis.
673 *Genome Res* 15(10):1451–1455.

674 56. Blankenberg D, et al. (2010) Galaxy: a web-based genome analysis tool for
675 experimentalists. *Curr Protoc Mol Biol* Chapter 19:Unit 19.10.1–21.

676 57. Goecks J, Nekrutenko A, Taylor J, Galaxy Team (2010) Galaxy: a comprehensive
677 approach for supporting accessible, reproducible, and transparent computational research
678 in the life sciences. *Genome Biol* 11(8):R86.

679 58. Li H, Durbin R (2009) Fast and accurate short read alignment with Burrows-Wheeler
680 transform. *Bioinformatics* 25(14):1754–1760.

681 59. Robinson JT, et al. (2011) Integrative genomics viewer. *Nat Biotechnol* 29(1):24–26.

682 60. Thorvaldsdóttir H, Robinson JT, Mesirov JP (2013) Integrative Genomics Viewer (IGV):
683 high-performance genomics data visualization and exploration. *Brief Bioinformatics*
684 14(2):178–192.

685 61. Garrison E, Marth G Haplotype-based variant detection from short-read sequencing.
686 *httpsarxivorgabsv* 2012.

687 62. Van der Auwera GA, et al. (2013) From FastQ data to high confidence variant calls: the
688 Genome Analysis Toolkit best practices pipeline. *Curr Protoc Bioinformatics* 43:11.10.1–
689 33.

690 63. Cingolani P, et al. (2012) Using *Drosophila melanogaster* as a Model for Genotoxic
691 Chemical Mutational Studies with a New Program, SnpSift. *Front Genet* 3:35.

692 64. Adjalley SH, Lee MCS, Fidock DA (2010) A method for rapid genetic integration into
693 *Plasmodium falciparum* utilizing mycobacteriophage Bxb1 integrase. *Methods Mol Biol*
694 634:87–100.

695 65. Spalding MD, Allary M, Gallagher JR, Prigge ST (2010) Validation of a modified method
696 for Bxb1 mycobacteriophage integrase-mediated recombination in *Plasmodium*

falciparum by localization of the H-protein of the glycine cleavage complex to the mitochondrion. *Mol Biochem Parasitol* 172(2):156–160.

Tables

Table 1. Summary of mutations identified by whole genome sequencing

Gene ID[a]	Description[b]	Base Call[c]			AA change	Population	Read Number[d]		%[e]	
		Position	WT	EMS			WT1	R	WT2	R
PF3D7_1128400	Geranylgeranyl pyrophosphate synthase (GGPPS)	682	T	A	S228T	019313R1	219	163	100	100
						019313R2	186	181	100	62.4

[a] PlasmoDB gene Identification number
[b] Basic gene description based on PlasmoDB functional assignments
[c] WT calls match 3D7 reference genome
[d] Read depth corresponding to WT call (IGV) and Mut call (SnpEff) respectively
[e] Percent of reads corresponding to WT call (IGV) and Mut call (SnpEff) respectively

Figures and figure legends

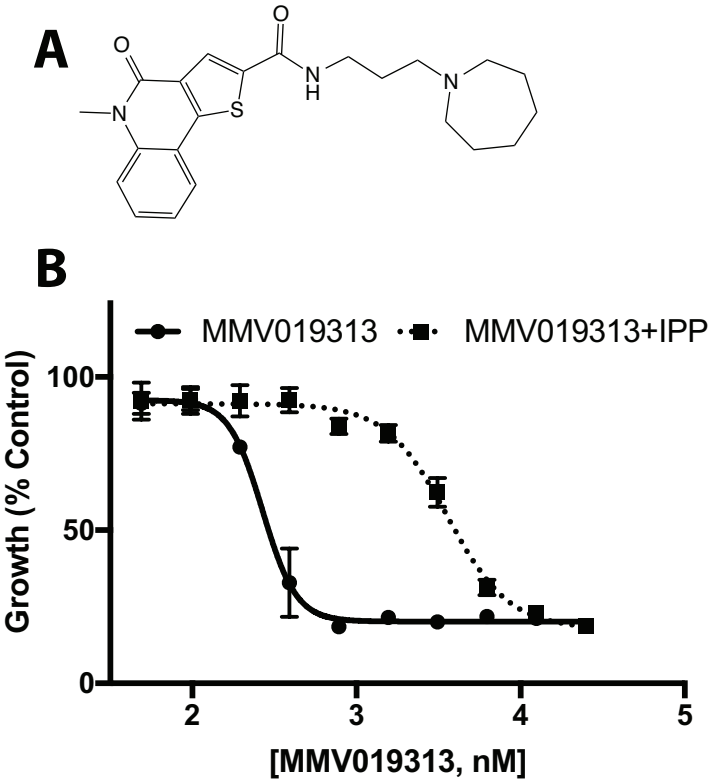

Figure 1. IPP rescues growth inhibition by MMV019313. A. The structure of MMV019313. **B.** EC_{50} curves in the absence (solid line) and presence (dotted line) of IPP. Parasitemia is normalized to that of an untreated control.

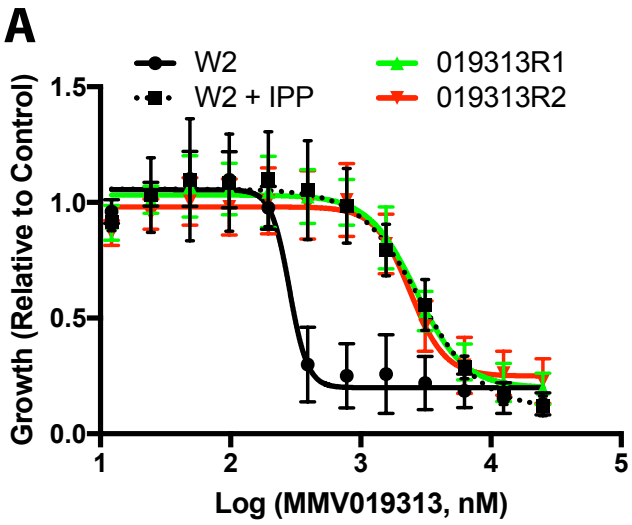

Strain	Fold Change EC_{50}
W2 + 200 µM IPP	10.06
019313R1	9.42
019313R2	8.45

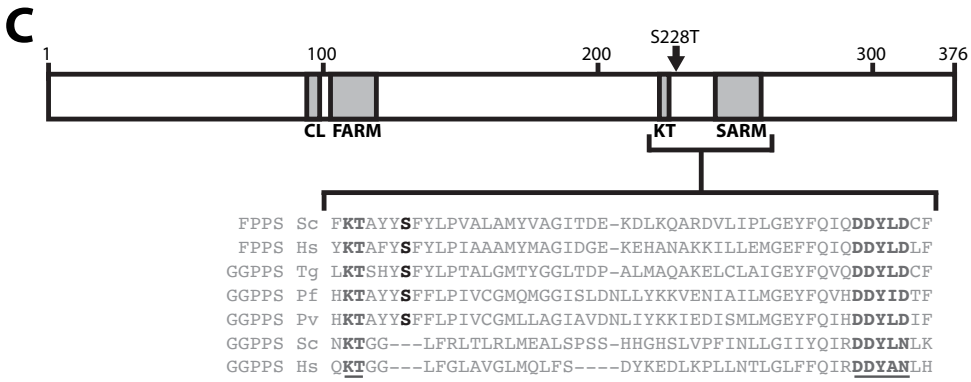

Figure 2. MMV019313-resistant parasites contain a mutation in the bifunctional farnesyl and geranylgeranyl diphosphate synthase. A. EC_{50} curves of parental W2 parasites alone (black, solid line) and with IPP supplementation (black, dotted line) and the two resistant populations (019313R1, red line, and 019313R2, green line) without IPP added. Fold change in EC_{50} compared to W2 parasites is shown in the right. **B**. Mutation determined by whole genome sequencing of resistant populations 019313R1 and 019313R2, highlighted in red **C.** Schematic of *Pf*FPPS/GGPPS protein. The S228T residue is highlighted in bold black while conserved KT and SARM residues are highlighted in bold grey and underlined.

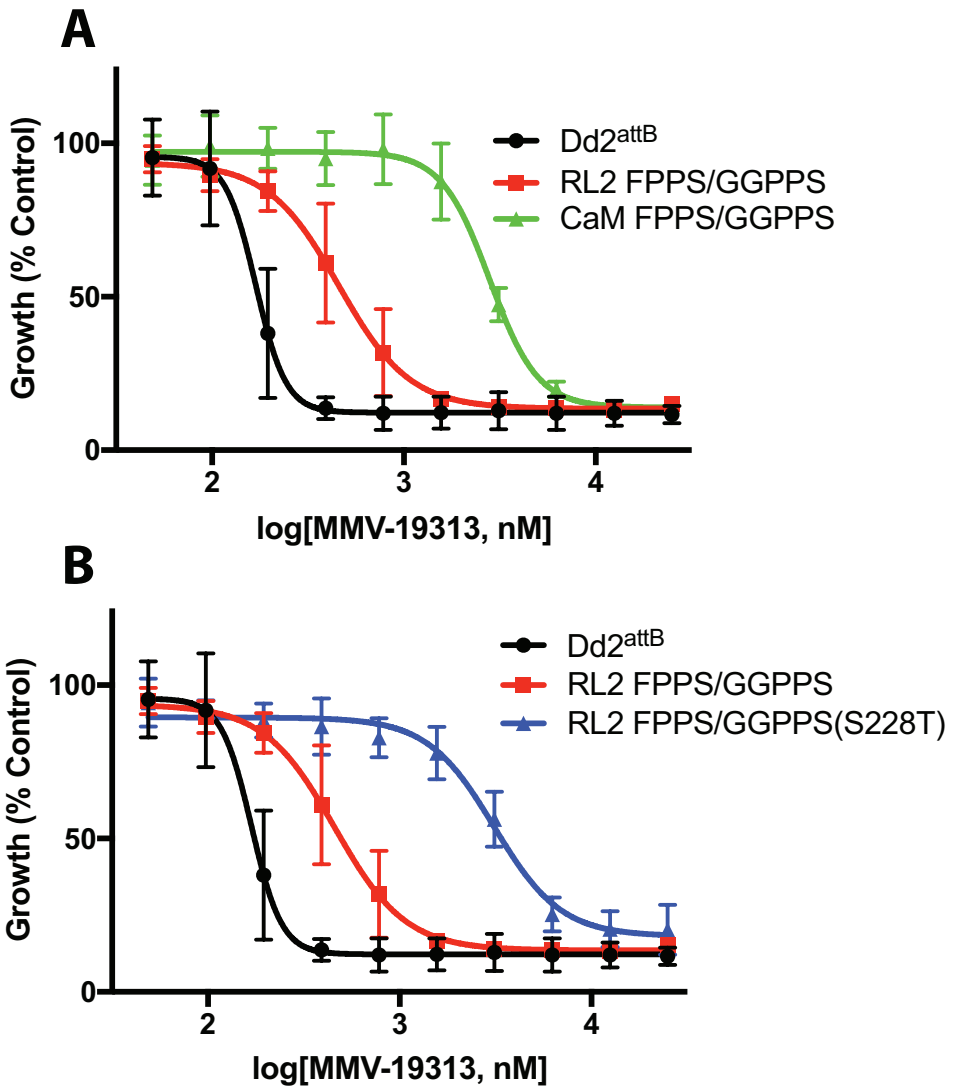

729
730 **Figure 3. Overexpression of WT and an S228T variant of *Pf*FPPS/GGPPS confer resistance**
731 **to MMV019313. A**. EC_{50} curves of MMV019313 against the parental $Dd2^{attB}$ parasites (black)
732 and parasites over-expressing FPPS/GGPPS-GFP under the RL2 (red) or CaM (green) promoter.
733 **B**. EC_{50} curves of MMV019313 against the parental $Dd2^{attB}$ parasites (black) and parasites over-
734 expressing wild type (red) or mutant (S228T, blue) FPPS/GGPPS-GFP under the RL2 promoter.
735

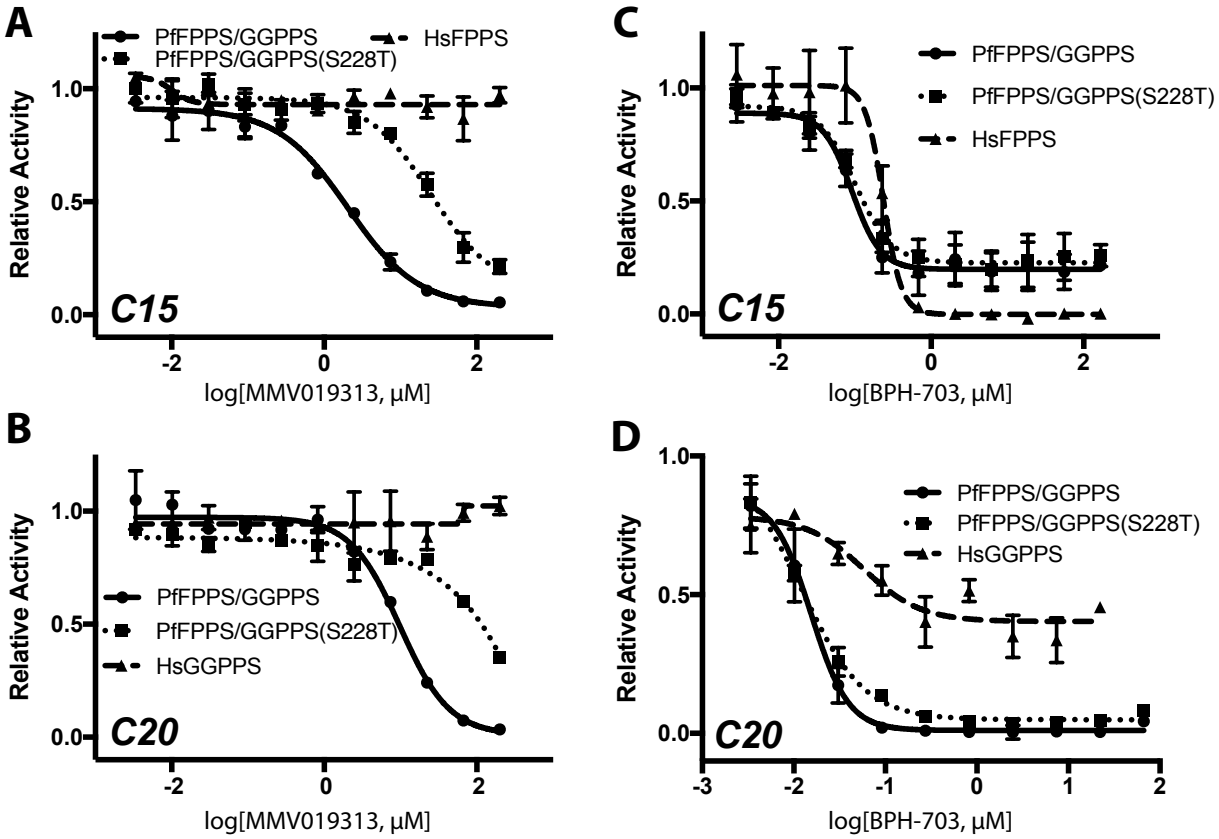

Figure 4. **MMV019313 has a specific and distinct mode-of-inhibition against purified *Pf*FPPS/GGPPS.** Dose-dependent inhibition of wild-type PfFPPS/GGPPS (solid), PfFPPS/GGPPS S228T variant (dotted), and either human FPPS or GGPPS (dashed) of **A**. FPP (C15) production by MMV019313, **B**. GGPP (C20) production by MMV010313, **C**. FPP (C15) production by BPH-703, and **D**. GGPP (C20) production by BPH-703. Partial inhibition of *Hs*GGPPS by BPH-703 was observed under k_{cat} conditions, while complete inhibition was observed under non-saturating conditions (**Figure S5**).